Journal of Applied Polymer Science

Influence of hydrogen bonding interaction on the damping properties of poly(*n*-butyl methacrylate)/small molecule hybrids

Xiaotong Yin, Chongyang Liu, Yu Lin, Aiguo Guan, Guozhang Wu
Shanghai Key Laboratory of Advanced Polymeric Materials, School of Materials Science & Engineering, East China University of Science & Technology, Shanghai 200237, People's Republic of China
Correspondence to: G. Wu (E-mail: wgz@ecust.edu.cn)

ABSTRACT: The hydrogen bonding interactions between poly(*n*-butyl methacrylate) and a series of low molecular weight phenols containing two to four hydroxyl groups with different steric effects were investigated by differential scanning calorimetry and Fourier-transform infrared spectroscopy. Results showed that the hydrogen bonding strength between the two components varies greatly according to the steric effects of the phenolic hydroxyl group. As the size of the group beside the hydroxyl increases, the hydrogen bond strength weakens. The glass transition temperature of binary hybrid systems was put into relation with the corresponding hydrogen bonding interaction strength. Strong hydrogen bonding strength increased T_g to higher values than that predicted by the linear additivity rule; by contrast, T_g of hybrid systems with weak hydrogen bonds showed linear changes. All of the samples showed linear variations at low concentrations of small molecules. The damping properties of five systems were analyzed by dynamic mechanical analysis. Either the loss factor or area of tan δ peak of the five systems increased compared with that of the pure polymer, thereby showing great improvements in the damping properties of the poly(*n*-butyl methacrylate)/small molecule hybrid material. © 2015 Wiley Periodicals, Inc. J. Appl. Polym. Sci. **2015**, *132*, 41954.

KEYWORDS: crystallization; differential scanning calorimetry; glass transition; property relations; structure

Received 3 September 2014; accepted 4 January 2015
DOI: 10.1002/app.41954

INTRODUCTION

The development of polymer/small molecule hybrid damping materials has received increased attention from researchers in recent years.[1–3] Studies have shown that the loss factor and TA value (area of tan δ peak) increase giantly with increasing number of small molecules in hybrid materials.[4–8] Using hydrogen bonds between small molecules and polymers to increase the damping property of hybrid materials presents infinite prospects for the manufacturing industry.[9,10] However, the influence of hydrogen bond interaction, including the strength and number of hydrogen bonds of the hybrid system, on damping properties remains unclear. Optimal selection of small molecules is also difficult to achieve because of the various structure and properties of small molecules.

Novel damping materials consist of polar polymers, such as chlorinated polyethylene, chlorinated polypropylene, and acrylate rubber, as well as some functional organic small molecules.[11,12] Studies have shown that addition of hindered amine or hindered phenol small molecules, such as *N*,*N*′-dicyclohexyl-benzothiazyl-2-sulfenamide or 3,9-bis{2-[3-(3-tert-butyl-4-hydroxy-5-methyl-phenyl)propionyloxy-1,1-dimethyl-ethyl]-2,4,8,10-tetraoxaspiro[5,5]undecane} (AO80), can greatly increase the peak height of tan δ because of internal friction between the polymer and small molecules and reversible hydrogen bond interaction in the blends, which consumes a large amount of mechanical energy to improve the damping performance of the resultant materials.[8,13] The glass transition temperatures (T_g) of hybrid materials can also be adjusted by changing the composition of the blends or regulating their intermolecular interactions to accommodate application condition.[14,15] Therefore, determination of the properties of small molecules as well as interactions between the polymer and small molecules, which exert significant influences on the damping performance of the materials, is worthy of discussion.

Matrix polymers must be considered according to the application and environment in which the material is to be applied. Polyacrylate materials have been proven to be an interesting class of materials because of their good processing and optical properties and thermal stability; these characteristics allow polyacrylate to be used as binders, textiles, or damping materials. Poly(*n*-butyl methacrylate) (PBMA) appears to be a good option for damping materials because the T_g of the polymer [25.4°C tested by differential scanning calorimetry (DSC)] occurs at approximately room temperature and the presence of local β relaxation (Johari Goldstein relaxation, β_{JG}) that can be observed at 30–80°C from dielectric spectroscopy may be

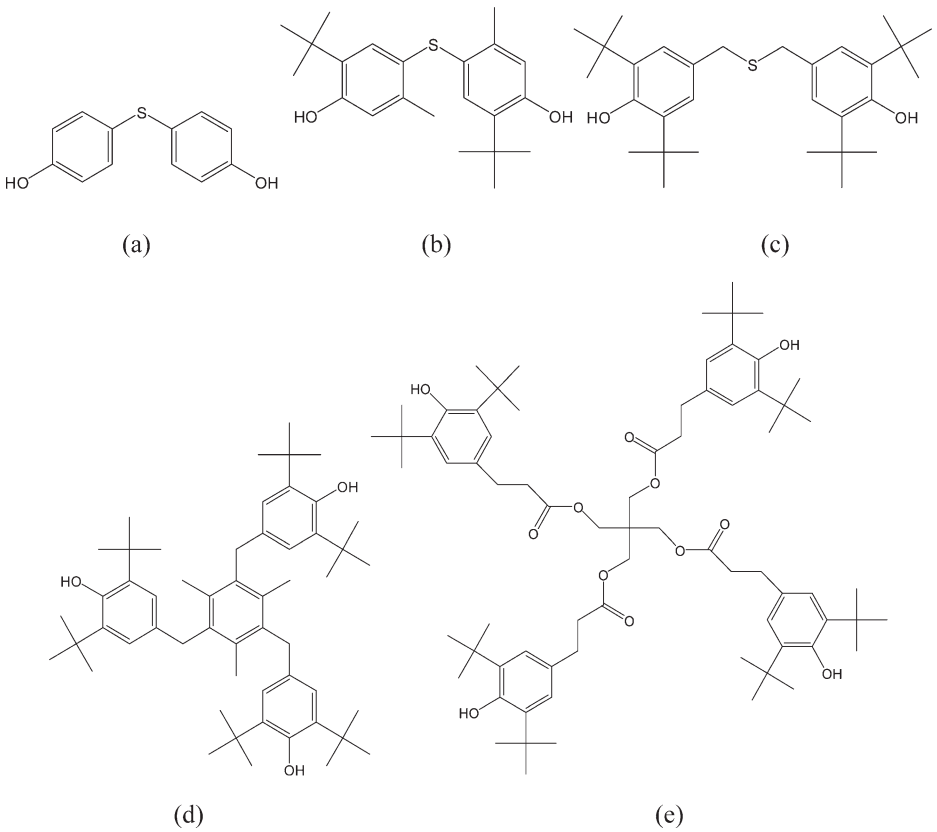

Figure 1. Chemical structures of (a) TDP, (b) AO300, (c) TBBP, (d) AO330, and (e) AO1010.

beneficial to its damping properties.[16,17] Studies have shown that addition of small molecules that can H-bond with polymers could affect the relaxation process of the matrix polymer.[18–20] Thus, the influence of hydrogen bonding interaction on β_{JG} relaxation of PBMA with addition of small molecules is also worth considering. The compatibility of polymer/small molecule hybrid systems is certainly an essential problem to be considered. Studies showed that polymer/small molecule systems behave an upper critical solution temperature phase behavior, miscible at low content of small molecules.[21] Further study of the phase diagram of the hybrids can be significant and meaningful.

In this study, five small molecules with different numbers of hydroxyl groups and levels of steric hindrance were used to explore the hydrogen bonding interactions and damping property of these hybrid systems. DSC and Fourier-transform infrared spectroscopy (FTIR) results showed that hydrogen bond interactions in small molecules may be distinguished according to their structures and self-association capacities, which have a direct influence on interactions between the polymer and small molecules and the T_g of polymer. The damping properties of five hybrid systems were also discussed and the systems under study proved to be high-performing materials in damping applications.

EXPERIMENTAL

Materials

PBMA ($M_w = 3.3 \times 10^6$ g/mol, PDI = 2.27, $T_g = 25.5 \pm 0.2$°C) was synthesized by solution polymerization in our laboratory. Small molecules of 4,4′-thio-bis(6-tert-butyl-*m*-methyl phenol) (AO300) and pentaerythritol tetrakis 3-(3,5-ditert-butyl-4-hydroxyphenyl)propionate (AO1010) were provided by Hongyuan Chemical Co. 1,3,5-Trimethyl-2,4,6-tris(3,5-di-tert-butyl-4-hydroxybenzyl) benzene (AO330) and 4,4′-thiodiphenol (TDP) were purchased from Aldrich. 4,4′-[Thiobis(methylene)]-bis[2,6-bis(1,1-dimethylethyl)phenol (TBBP) was provided by Mitsubishi Chemical Corporation Japan. Figure 1 illustrates the chemical structures of these molecules.

Sample Preparation

Films of small molecules and PBMA were prepared by solution casting; here, the small molecule content of the films was varied from 10 phr to 300 phr. Small molecules and PBMA with different ratios were dissolved in acetone at a given concentration of 10 wt %. Samples were dried at room temperature for 3 days to volatilize the solvent. They were then heated at 120°C for 2 h in a vacuum oven to remove the remaining solvent. All samples were placed under vacuum for a week before testing was performed.

Differential Scanning Calorimetry

The T_g and melting temperature (T_m) of the samples were determined using a TA Instruments Q200 differential scanning calorimeter under purging with dry nitrogen at a rate of 40 mL/min. Temperatures were calibrated using an indium standard. Samples were heated from −30°C to 200°C at a heating rate of 10°C/min and maintained at 200°C for 5 min to eliminate thermal history before cooling down to −30°C at

10°C/min. Subsequently, samples were reheated to 200°C at a heating rate of 10°C/min to obtain the T_g.

Fourier-Transform Infrared Spectroscopy

Infrared spectra were obtained using a Nicolet 5700 IR spectrometer at room temperature. The FTIR spectra of all of the samples were recorded from 4000 cm^{-1} to 400 cm^{-1} with 64 scans at a resolution of 0.9 cm^{-1}. Samples were prepared by depositing sample solutions onto KBr windows, after which the solvent was evaporated at room temperature.

Dynamic Mechanical Analysis

Dynamic thermal mechanical measurements were conducted using a TA Instruments Q800 dynamic mechanical analyzer under dry nitrogen purging. Using the tension mode at a constant frequency of 1 Hz and temperature range of −20°C to 120°C with a heating rate of 3°C/min, all samples were molten

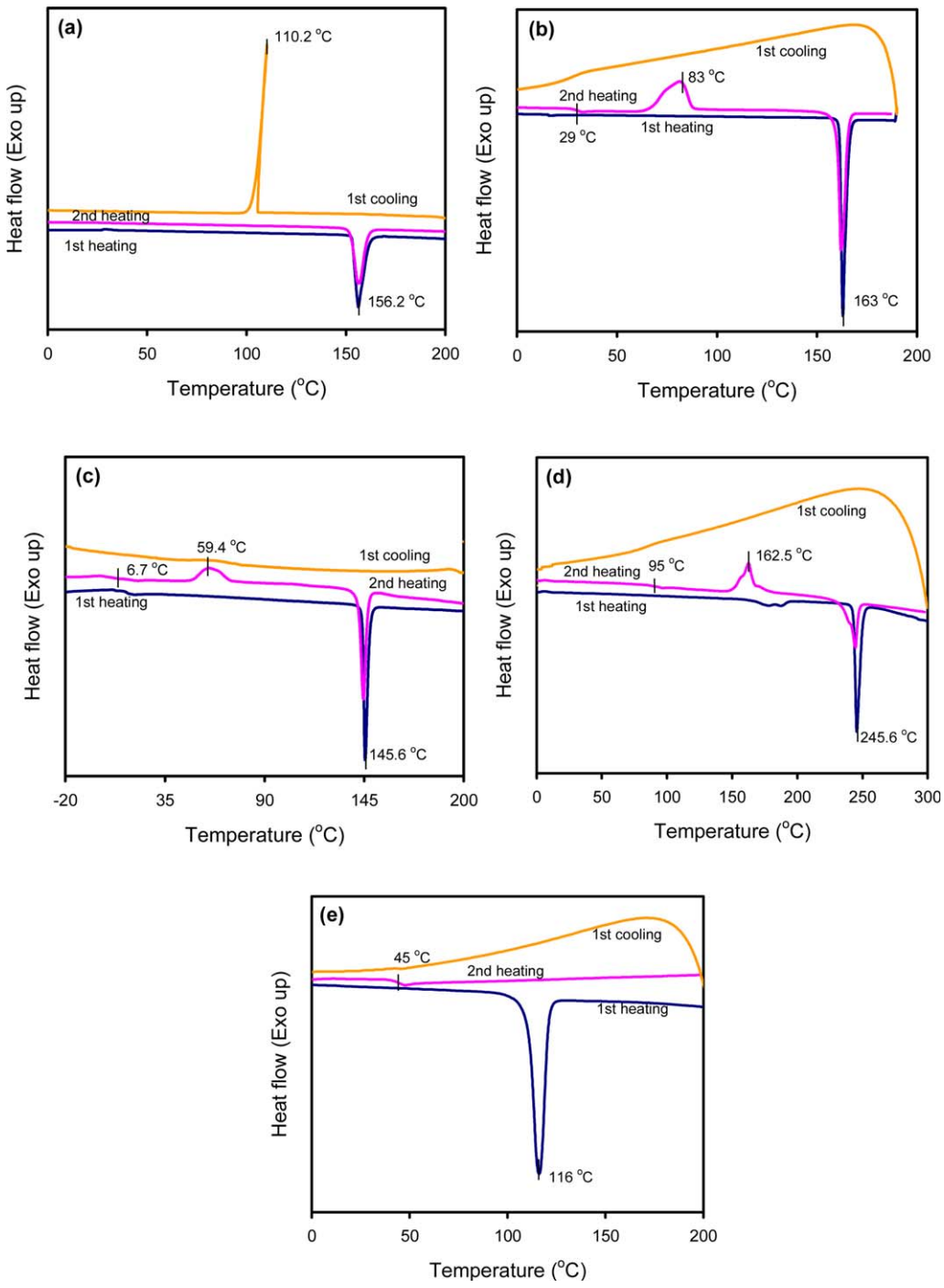

Figure 2. DSC curves of (a) TDP, (b) AO300, (c) TBBP, (d) AO330, and (e) AO1010. [Color figure can be viewed in the online issue, which is available at wileyonlinelibrary.com.]

and compression-molded for 15 min under a pressure of 10 MPa before quenching at 10°C. All samples were dried under vacuum at room temperature for a week before testing.

RESULTS AND DISCUSSION

Hydrogen Bonding Interactions Between Small Molecules

DSC measurements were used to detect the T_g and T_m of small molecules, as well as possible crystallization during cooling, cold-crystallization, and melting in the second heating. Figure 2 shows the DSC curves of a series of small molecules; in this figure, three types of crystallization process may be observed, and each process presents a typical crystal type.

All of the small molecules show a melting process during the first heating because most small molecules tend to exist in a crystalline state at room temperature. Figure 2(a) describes the strong crystalline ability of small molecules that undergo crystallization during cooling, such as TDP. Figure 2(b,c) shows molecules with relatively weaker crystalline ability featuring

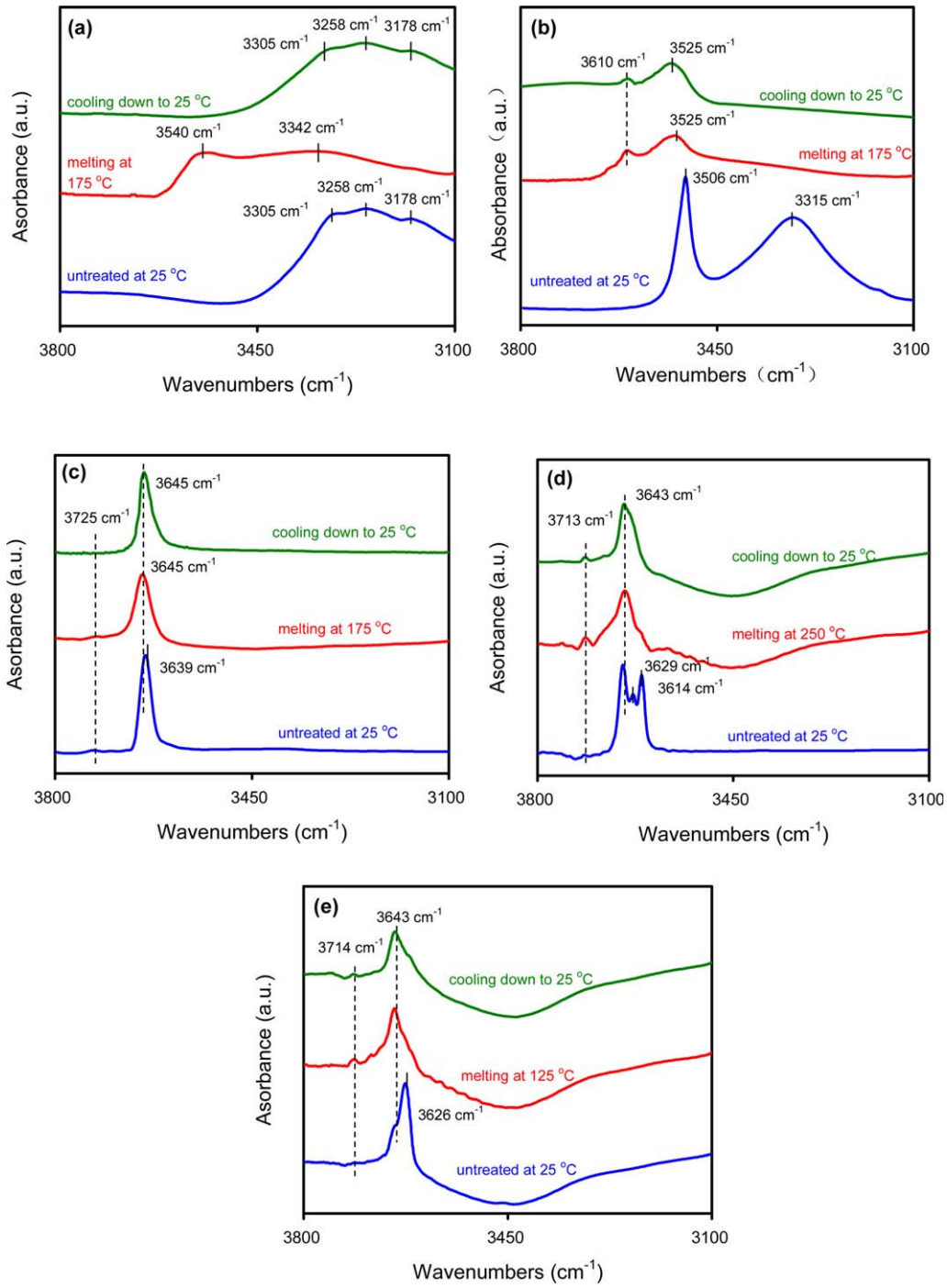

Figure 3. FTIR spectra of (a) TDP, (b) AO300, (c) TBBP, (d) AO330, and (e) AO1010 untreated at 25°C, melting, cooling down to 25°C. [Color figure can be viewed in the online issue, which is available at wileyonlinelibrary.com.]

Table I. Peak Positions of Different Types of Hydroxyls in the Small Molecules (±1 cm^{-1}) and Some Parameters of These Molecules

	TDP	AO300	TBBP	AO330	AO1010
$\nu_{HB\text{-}crystal}$	3258, 3178	3315	3639	3629, 3614	3626
$\nu_{HB\text{-}amorphous}$	3305	3506	3645	3643	3643
ν_{free}	3540	3610	3725	3713	3714
$\nu_{free}-\nu_{HB\text{-}amorphous}$	235	104	80	70	71
$\nu_{free}-\nu_{HB\text{-}crystal}$	282, 362	295	86	84, 99	88
Self-association	Strong	Moderate	Weak	Weak	Weak
T_g	N/A	29°C	6.7°C	95°C	45°C
T_m	156.2°C	163°C	145.6°C	245.6°C	116°C

cold-crystallization during the second heating, such as AO300 and TBBP. This is because the steric effects in these two molecules related to phenolic hydroxyls are stronger compared with those in TDP, which may lead to a decrease in crystalline ability. The steric effects of phenolic hydroxyls in TBBP, AO330 and AO1010 are nearly the same, but the number of hydroxyl in the latter two molecules is higher than that in TBBP. Larger numbers of hydroxyl groups could lead to a denser hydrogen bond network, which can cause a decline in mobility and regularity. Therefore, the crystal capacity of these two molecules is weakened. In fact, AO1010 shows neither cooling crystallization nor cold-crystallization. Therefore, the intramolecular hydrogen bond interactions may explain the different crystallization behavior of small molecules.

To confirm our hypothesis, in situ FTIR was used to detect the peak position change in hydroxyls with different states of small molecules. A red-shift phenomenon[22] may occur when a free hydroxyl (ν_{free}, position of free hydroxyl) is H-bonded to another group ($\nu_{H\text{-}bonded}$, position of hydrogen-bonded hydroxyl). As the hydrogen bond interaction becomes strong, the red-shift phenomenon ($\Delta\nu$, position change between free hydroxyl and hydrogen-bonded hydroxyl) becomes obvious.[23,24] Therefore, three states of small molecules were tested to help understand the hydrogen bonding strength in small molecules. All of the samples were dehydrated in vacuum at 110°C before testing, and the test conditions applied were similar to those used for DSC.

In Figure 3, the bottom curve describes the untreated sample tested at room temperature, the middle curve describes the melting state of small molecule, and the top curve describes the spectra of samples that have been cooled down from melting temperature to room temperature. Figure 3(a) shows that TDP has three prominent O–H stretching peaks that correspond to the hydrogen-bonded (H-bonded) hydroxyl in amorphous TDP at 3305 cm^{-1} and two H-bonded hydroxyl in crystal TDP at 3258 cm^{-1} and 3178 cm^{-1}. After melting at 175°C for 5 min, the peaks of crystal TDP disappear. A new peak then appears at 3540 cm^{-1}, which is responsible for free O–H absorbance peak, and the $(O\text{–}H)_{amorphous}$ peak shifts to a high wavenumber because of high temperature. The position change ($\Delta\nu$) between free hydroxyl and H-bonded hydroxyl of amorphous TDP accounts for the strength of hydrogen bond in TDP, which is 235 cm^{-1}, thus, showing a strong intramolecular interaction. The three hydroxyl peaks of TDP reappear after cooling from melting state to room temperature which is agreed with DSC result that TDP crystallizes during cooling process.

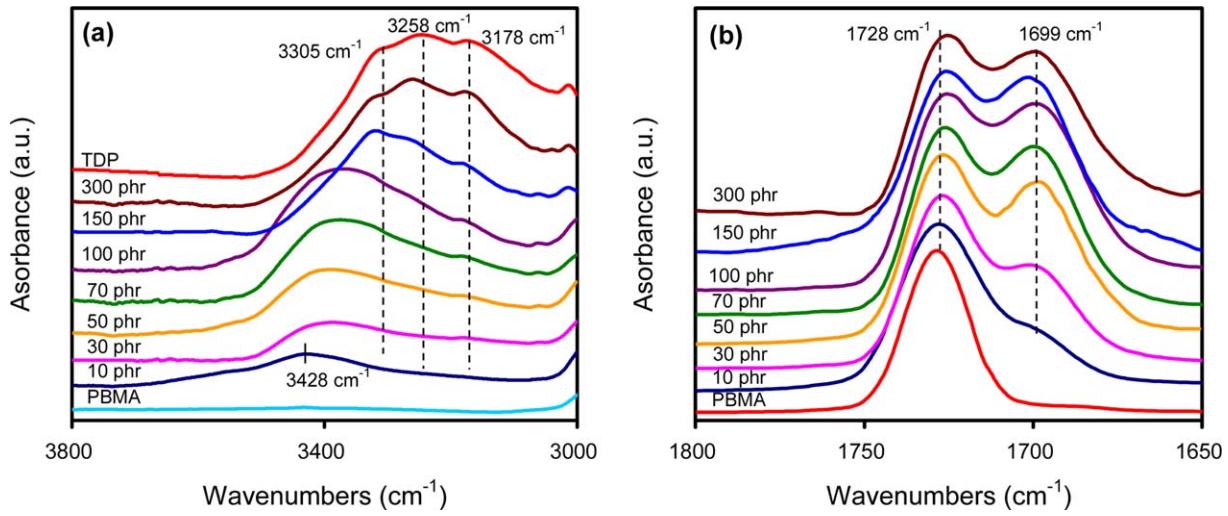

Figure 4. FTIR spectra of hydroxyl vibration region (a) and carbonyl vibration region (b) of PBMA/TDP system with different loadings of TDP. [Color figure can be viewed in the online issue, which is available at wileyonlinelibrary.com.]

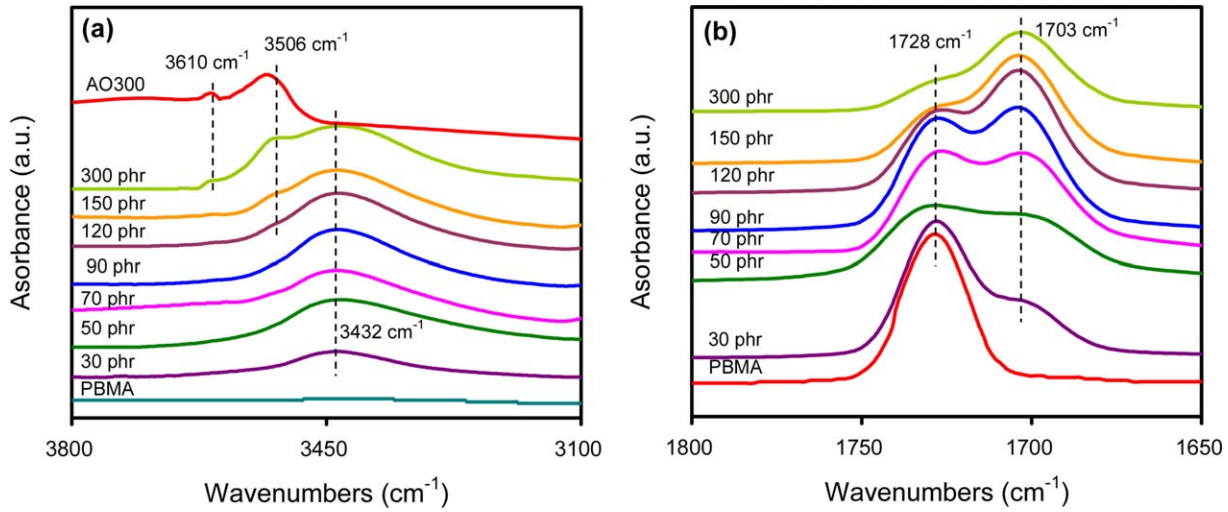

Figure 5. FTIR spectra of hydroxyl vibration region (a) and carbonyl vibration region (b) of PBMA/AO300 with different loadings of AO300. [Color figure can be viewed in the online issue, which is available at wileyonlinelibrary.com.]

As for AO300 [Figure 3(b)], two O–H peaks exist at 3506 cm^{-1} and 3315 cm^{-1}, which represent the H-bonded hydroxyl of amorphous and crystalline AO300, respectively. The crystal peak disappears after melting at 175°C, and a new peak appears at 3610 cm^{-1}, which is the free hydroxyl of AO300. The cooling down spectrum shows a weak free O–H peak and a $(O–H)_{amorphous}$ peak with no crystal in small molecule, which corresponds with the DSC result that AO300 does not crystallize during cooling.

In the case of TBBP, AO330, and AO1010, the hydroxyl peaks of crystalline and amorphous state are extremely close, which indicates a similar hydroxyl structure feature in crystalline and amorphous state of small molecule. The similar results can be observed when the $(O–H)_{crystal}$ peaks disappear above melting point of the small molecules and new peaks assigned to free hydroxyl emerge at 3725 cm^{-1}, 3713 cm^{-1}, and 3714 cm^{-1}. Both the cooling down spectra show no sign of $(O–H)_{crystal}$ peaks agreed with DSC results that these small molecules do not crystallize during temperature-falling period. It should be noticed that the assignment of $(O–H)_{crystal}$ peak of TBBP is difficult due to the fact that peaks of crystal and amorphous TBBP can be overlapped at the point.

The relative hydrogen bond strength that reflects the self-association capacity could be characterized by Δv_a (position change between free hydroxyl and H-bonded hydroxyl of amorphous small molecule), as shown in Table I. In such case, as the steric effects of phenolic hydroxyl increase in the order of TDP, AO300, and TBBP, Δv_a of three molecules decreased. Δv_c (position change between free hydroxyl and H-bonded hydroxyl of crystal small molecule) could reflect the crystalline ability of small molecules and it is decreasing as well. Therefore, AO300 and TBBP have a cold-crystallization process, whereas TDP shows a cooling crystallization.

Δv_a and Δv_c of TBBP, AO330, and AO1010 remain almost the same with the similar steric hindrance. In such circumstance,

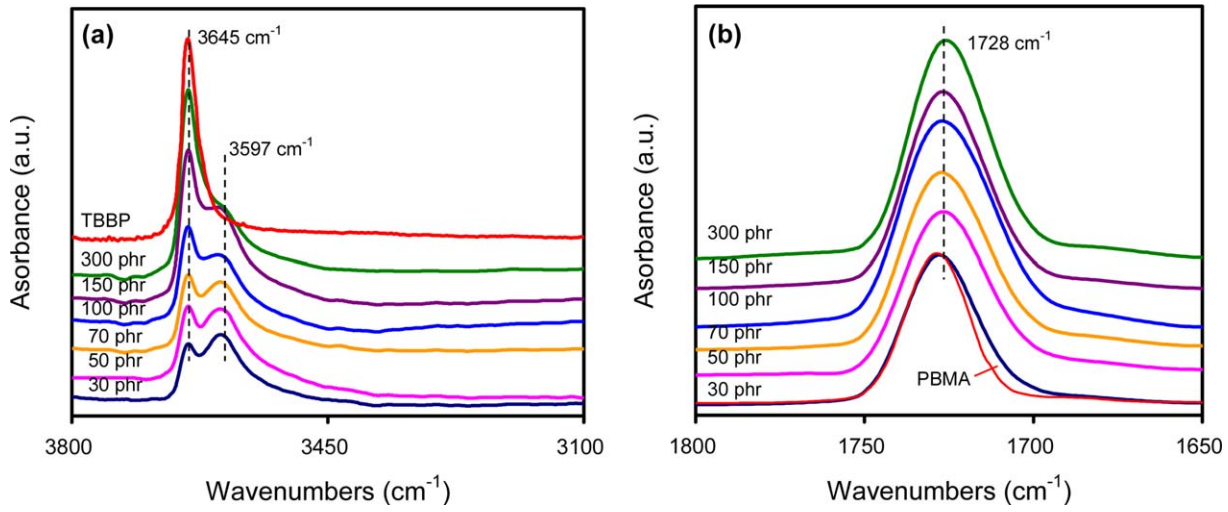

Figure 6. FTIR spectra of hydroxyl vibration region (a) and carbonyl vibration region (b) of PBMA/TBBP with different loadings of TBBP. [Color figure can be viewed in the online issue, which is available at wileyonlinelibrary.com.]

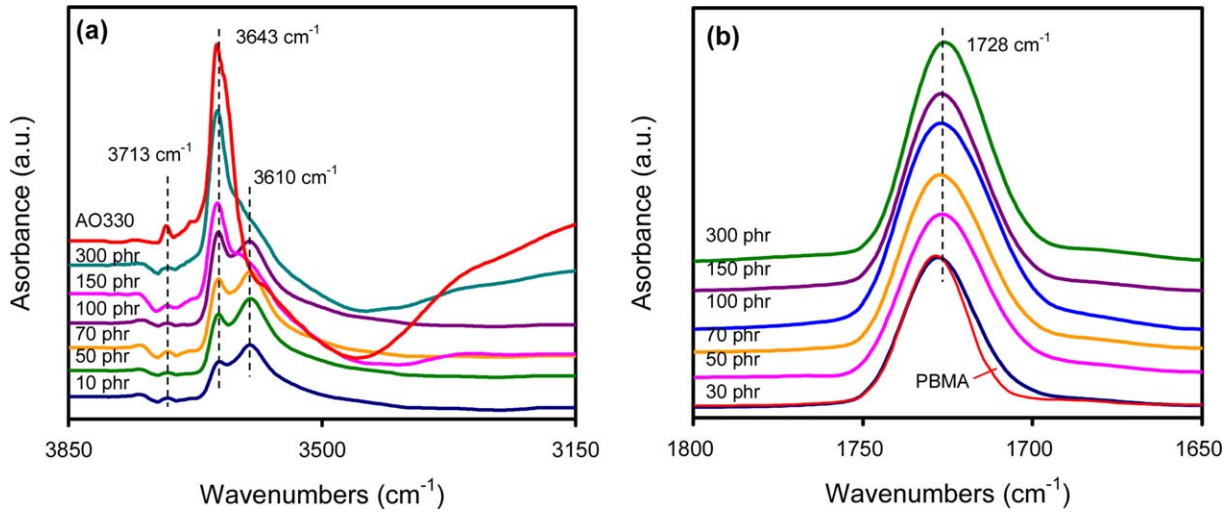

Figure 7. FTIR spectra of hydroxyl vibration region (a) and carbonyl vibration region (b) of PBMA/AO330 with different loadings of AO330. [Color figure can be viewed in the online issue, which is available at wileyonlinelibrary.com.]

the bulk size of H-bonded small molecules plays a leading role in the crystalline ability. As the size of these three small molecules increases, their mobility declines, thereby aggravating the difficulty to crystallize. Furthermore, the number of phenolic hydroxyl increases that leads to an irregular hydrogen bonding network, which also makes the molecule difficult to range into the crystal lattice. As a result, AO1010 shows no crystallization in the DSC curves, and AO330 needs a higher temperature to crystallize than TBBP.

The diversity of small molecules will directly affect the interaction between the polymer and small molecules and lead to different segmental mobility, as reflected in the T_g of the polymer hybrids.

Interplay Between the Polymer and Small Molecules and Its Influence on T_g

For a hydrogen bond network, FTIR could detect the type and strength of hydrogen bonding between the components of the mixtures through an examination of the O–H stretching region from 3800 cm^{-1} to 3100 cm^{-1} and C═O stretching region from 1800 cm^{-1} to 1650 cm^{-1}.

Figure 4 presents the FTIR spectra of PBMA/TDP system with different loadings of TDP in the hydroxyl and carbonyl vibration regions. In Figure 4(a), given the molecule loading with polymer, a strong band appears near 3428 cm^{-1} that is characterized as the hydroxyl of TDP H-bonded with the carbonyl of PBMA. Meanwhile, the carbonyl group of PBMA is H-bonded to hydroxyl, which appears a new peak near 1699 cm^{-1}, and the other free carbonyl of PBMA remains in 1728 cm^{-1}. The H-bonded hydroxyl of TDP locates at lower wavenumber than hydroxyl H-bonded with polymer; thus, the self-associated hydrogen bonding strength of TDP is stronger than the intermolecular hydrogen bonds between TDP and polymer. The same results are confirmed by other scientists.[25] As the content of TDP increases, the peak of hydroxyl group shifts to a low wavenumber closing to the H-bonded hydroxyl of TDP, as a result of the agglomeration of TDP. As the content of TDP increase, the absorbance peak of H-bonded carbonyl increases, whereas the free carbonyl peak decreases. However, given that the loading of TDP is high, the H-bonded carbonyl content drops and the hydroxyl of TDP itself becomes clear, which suggests a strong self-association force of TDP.

In case of PBMA/AO300 mixtures, no crystal form of AO300 appears in the measurement process. Figure 5 shows that the number of H-bonded either hydroxyl or carbonyl increases with the content of AO300. A new band is also observed near 3506 cm^{-1} when the concentration of AO300 exceeds 120 phr. Therefore, the number of H-bonded hydroxyl of AO300 with carbonyl of PBMA is saturated and causes the hydroxyl H-bonded between small molecules itself. The H-bonded hydroxyl groups do not aggregate to form crystals but disperse in the polymer, which proves that the interaction between small molecules in AO300 is weaker than that in TDP. As the content of AO300 increases, a weak peak appears at 3610 cm^{-1} assigned to the free hydroxyl of AO300. The appearance of free hydroxyl is influenced by the steric hindrance of phenolic hydroxyl. Thus, a small amount of hydroxyl groups cannot H-bonded with neither the polymer nor the other small molecules.

As the isobutyl beside hydroxyl group increases, the hydrogen bond strength between the polymer and small molecules substantially decreases, as shown in Figure 6. Unlike the first two systems, two peaks exist at the hydroxyl vibration region. The peak located at a high wavenumber is assigned to the H-bonded hydroxyl of TBBP, and the other one is the hydroxyl of TBBP H-bonded with C═O group of PBMA. Only partial of the hydroxyl groups can be H-bonded with polymer because of the huge steric hindrance beside two sides of the phenolic hydroxyl. The carbonyl vibration region shows only one clear peak, and the peak maximal position remains at 1728 cm^{-1}. However, the peak is obviously broad at the low-wavenumber region, which suggests a weak hydrogen bonding interaction between C═O group and O–H group.

In terms of PBMA/AO330 and PBMA/AO1010, a slightly broad band exists at the low wavenumber in the carbonyl region in

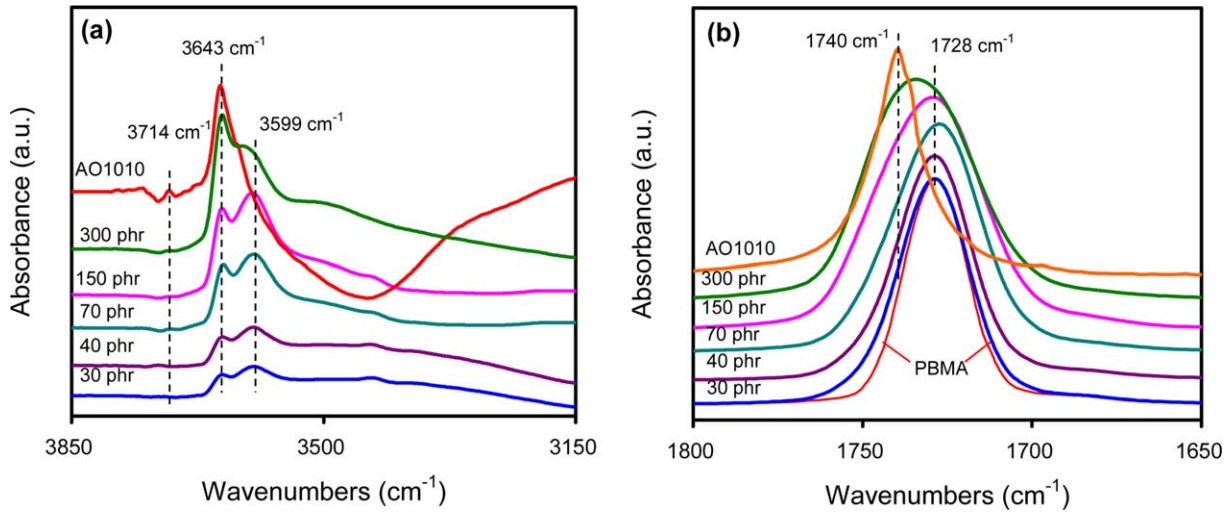

Figure 8. FTIR spectra of hydroxyl vibration region (a) and carbonyl vibration region (b) of PBMA/AO1010 with different loadings of AO1010. [Color figure can be viewed in the online issue, which is available at wileyonlinelibrary.com.]

Figures 7(b) and 8(b), which resembles the PBMA/TBBP system. The free hydroxyl in AO330 and AO1010 can be barely observed at 3713 cm^{-1} and 3714 cm^{-1}, respectively. As the hydroxyl group in AO330 increases, the number of hydrogen bond between PBMA and AO330 is higher compared to that of PBMA/TBBP system. Figure 7(b) also shows that the broad of main peak at a low wavenumber is clearer compared with PBMA/TBBP system, accounting for the assumption. However, the number of hydrogen bond in PBMA/AO1010 system does not increase as expected. The bulk size of H-bonded small molecules increases the difficulty to form other hydrogen bonds in the same small molecule, thereby leading to a decrease in the number of hydrogen bonds in the PBMA/AO1010 system. It should be mentioned that, due to the overlapping of the carbonyl group of AO1010 at 1740 cm^{-1} with PBMA at 1720 cm^{-1}, the absorbance peak of PBMA/AO1010 blends shown in Figure 8(b) becomes broader at the high-wavenumber side with increasing AO1010 loadings.

The different interactions between the polymer and small molecules should lead to different behavior of the segmental relaxation, which is apparently exhibited in the T_g of the hybrid materials.

Figure 9 presents T_gs of five binary hybrid materials with different loadings of small molecules. T_gs of AO300, TBBP, AO330, and AO1010 tested by DSC are 29°C, 6.7°C, 94.5°C, and 45°C, respectively. However, T_g of TDP cannot be tested or obtained elsewhere because of the strong crystalline ability and therefore, we can not discuss the influence of H-bonding strength on T_g for TDP-filled mixtures. For PBMA/AO300 blends [Figure 9(a)], it displays higher T_gs than the ones predicted by Fox equation, which is mostly caused by the formation of strong intermolecular hydrogen bonding between polymer andAO300.[12,26] The AO300 H-bonded to the carbonyl group of the PBMA acts like side chains and thereby increases the rigidity of the pendent group, leading to the increase in

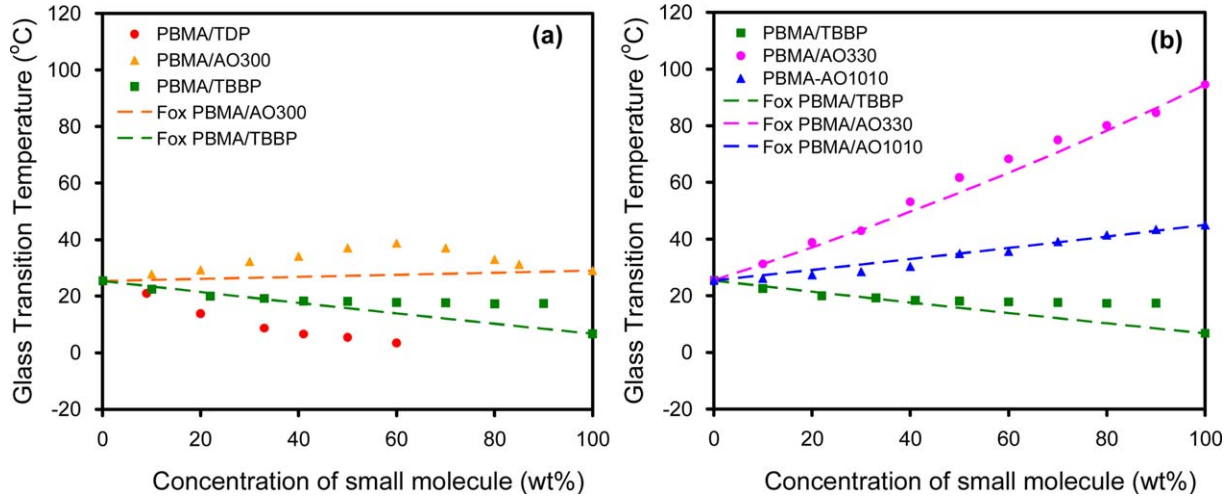

Figure 9. Glass transition temperatures of five hybrid systems with different loadings of small molecules, experimental result (spots), predicted by Fox Equation (dashes). [Color figure can be viewed in the online issue, which is available at wileyonlinelibrary.com.]

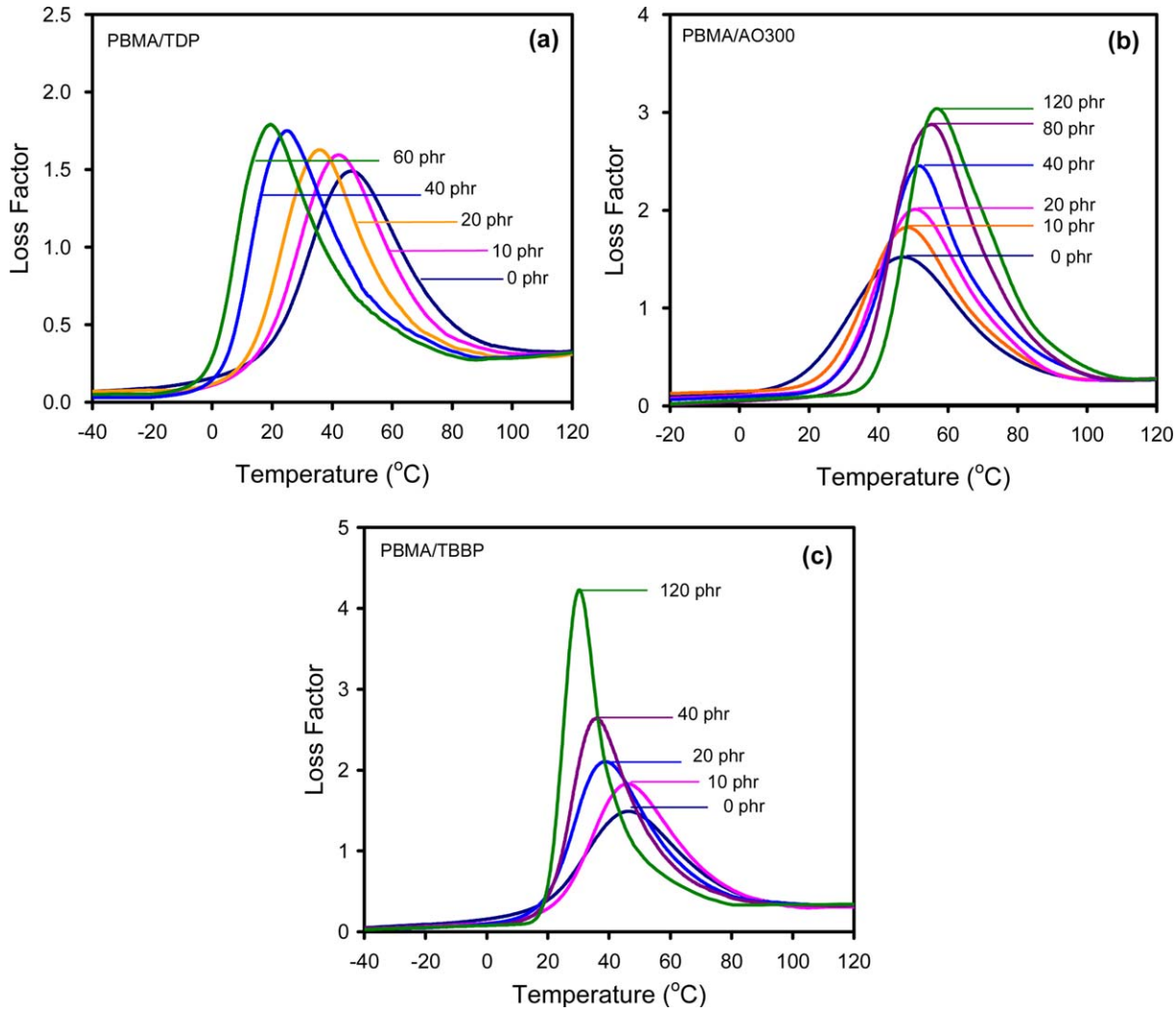

Figure 10. Temperature dependence of tan δ of (a) PBMA/TDP, (b) PBMA/AO300, and (c) PBMA/TBBP hybrid systems. [Color figure can be viewed in the online issue, which is available at wileyonlinelibrary.com.]

T_g. As the content of AO300 exceeds 60 wt %, the small molecules begin to aggregate together by hydroxyls H-bonding and DSC test confirms that a melting process appears at loadings of AO300 higher than that value. This suggests the decrease in T_g at high loadings because of the small molecule self-association.

In the case of PBMA/TBBP, PBMA/AO330, and PBMA/AO1010 hybrids with the similar steric hindrance of phenolic hydroxyl, the hydrogen bonding interaction strengths between the polymer and small molecules are almost the same and relatively weak. The T_gs of three systems fit well with the predicted results by Fox equation.

Damping Properties of Polymer/Small Molecule Hybrid System

The damping property of materials could be evaluated by the peak height (tan δ_{peak}) and peak area (TA value) of temperature dependence of loss factor (tan δ) curve. Five polymer/small molecule hybrid materials were prepared and their damping properties are discussed.

Figure 10 shows the tan δ curves of three hybrid systems with different steric hindrance of hydroxyl groups of small molecules. It can be seen that hybrids with strong hydrogen-bond interaction (between polymer and small molecules) as well as strong self-association of small molecule show litter improving in tan δ, such as PBMA/TDP hybrid. The self-association of TDP is stronger than the interaction between polymer and TDP as seen in Figure 4, which makes litter contribution on damping property. Hybrids with moderate hydrogen-bond interaction and self-association of small molecule show better improvement in tan δ, such as PBMA/AO300 hybrid. Hybrids with weak hydrogen-bond interaction and self-association of small molecules show largest improvement in tan δ, such as PBMA/TBBP hybrid. In the latter two systems, interaction between polymer and small molecules is stronger than the self-association of small molecules. By drawing a conclusion, the interaction between small molecules goes against the damping property of hybrids while the interaction between polymer and small molecules is beneficial to the damping property of hybrids.

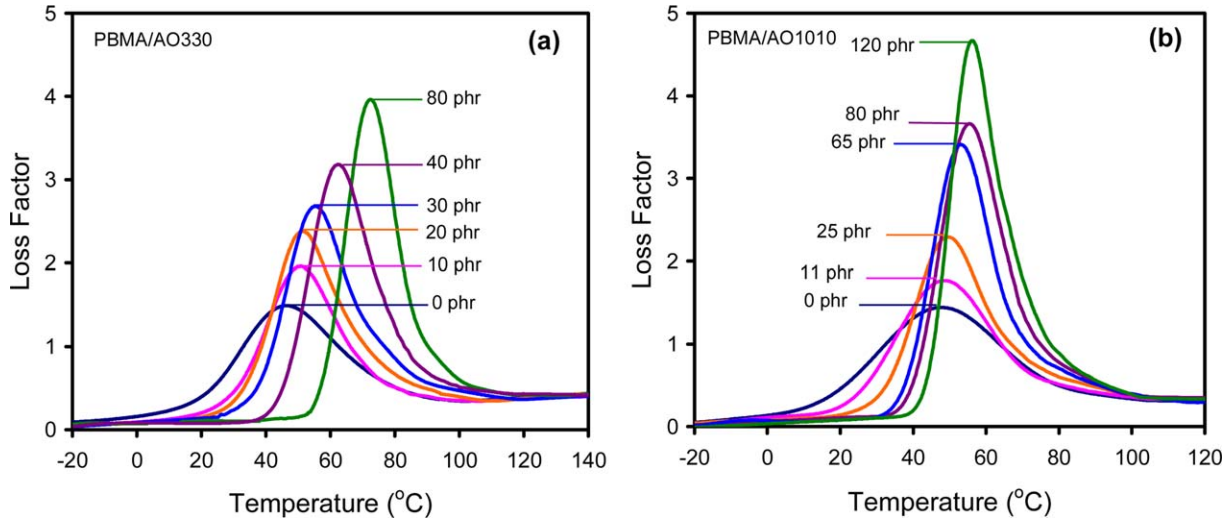

Figure 11. Temperature dependence of tan δ of (a) PBMA/AO330 and (b) PBMA/AO1010 hybrid systems. [Color figure can be viewed in the online issue, which is available at wileyonlinelibrary.com.]

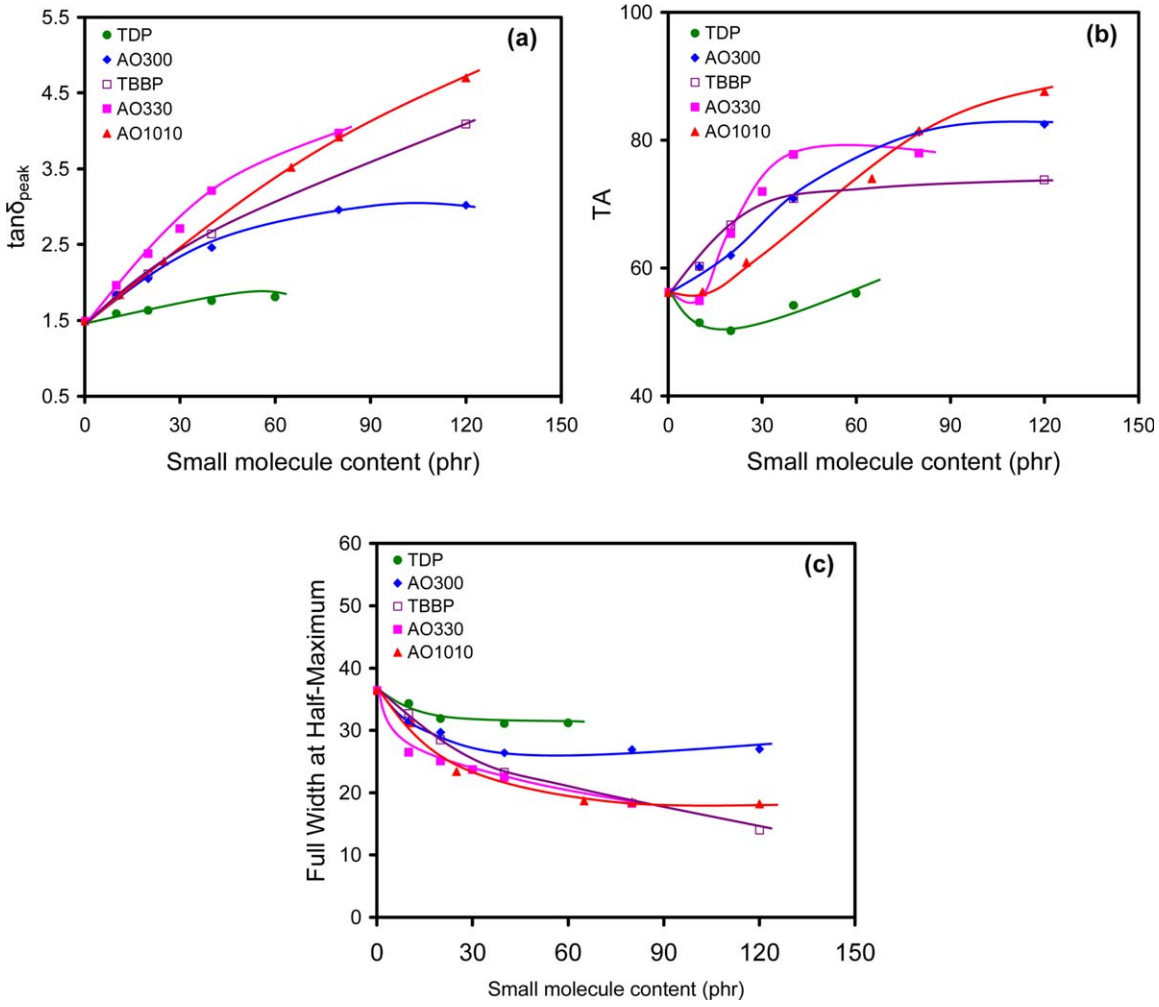

Figure 12. Damping parameters of five PBMA/small molecule hybrid systems with different small molecule contents, (a) tan δ_{peak}, (b) TA values, and (c) full width at half-maximum. [Color figure can be viewed in the online issue, which is available at wileyonlinelibrary.com.]

Table II. Damping Parameters of Five Hybrid Materials with Different Loadings of Small Molecules

Small molecule	Content (phr)	tan δ_{peak} temperature (°C)	tan δ_{peak} value (±0.02)	Full width at half-maximum (±0.2°C)	TA value (±0.2)	TA improvement in percentage
TDP	0	46.3	1.49	36.4	56.2	0
	10	42.2	1.59	34.3	51.5	−8.4
	20	35.8	1.63	31.9	50.2	−10.7
	40	24.9	1.76	31.1	54.2	−3.6
	60	19.4	1.81	31.2	56.1	−0.2
AO300	10	47.6	1.84	31.4	60.2	7.1
	20	50.1	2.05	29.7	62.0	10.3
	40	51.9	2.46	26.4	70.9	26.2
	80	54.1	2.96	26.9	81.3	44.7
	120	55.0	3.02	27.0	82.5	46.8
TBBP	10	46.2	1.83	32.7	60.3	7.3
	20	38.8	2.11	28.5	66.8	18.9
	40	36.0	2.64	23.3	70.9	26.2
	120	30.3	4.09	14.0	73.8	31.3
AO330	10	50.8	1.96	26.5	54.9	−2.3
	20	51.4	2.38	25.1	65.4	16.4
	30	55.0	2.71	23.7	72.0	28.1
	40	61.4	3.21	22.5	77.8	38.4
	80	70.7	3.97	18.3	78.0	38.8
AO1010	11	47.1	1.84	31.2	56.3	0.2
	25	49.1	2.28	23.4	60.9	8.4
	65	52.5	3.52	18.7	74.0	31.7
	80	54.5	3.92	18.5	81.5	45.0
	120	56.0	4.70	18.2	87.6	55.9

Figure 11 shows the tan δ curves of similar hydrogen-bond interaction systems with different hydroxyl groups of small molecules. Addition of these small molecules rapidly increased tan δ_{peak} to high values just like PBMA/TBBP hybrid system. However, the number of phenolic hydroxyls is different, which may change the hydrogen bond density between the polymer and small molecules in the systems.

The damping parameters of the five systems are presented in Figure 12 and Table II. The peak height of tan δ of five systems can be seen in Figure 12(a). The peak height variation is related to the hydrogen-bond density and interaction strength which can be reflected in T_g of the system. With 40 phr loading of small molecules, the peak height of five system decreases in the order of AO330, AO1010, TBBP, AO300, and TDP, similar order with T_g of five hybrids as seen in Table II.

TA value increases by the addition of small molecules in most hybrids as seen in Figure 12(b), although there is some decrease with low content of small molecules. However, as the content of small molecules further increases, TA increases in a slow way, except for the PBMA/AO1010 system. This is because at high loadings, the number of hydrogen bonding between the polymer and the small molecules become saturated due to the steric hindrance and subsequently small molecules crystallize at their rich region. The melting process of small molecules observed from DSC curves proves the existence of crystals. In the PBMA/AO1010 system, the weak intramolecular interaction and crystalline ability of AO1010 impairs the self-aggregation and crystallization of small molecule, thereby leading to constant increase in TA values with addition of AO1010.

The narrow down of peak width can be observed in all the systems as seen in Figure 12(c), which may influence the decrease in TA with low content of small molecules. It is possibly attributed to two factors. First, addition of small molecules can lead to a sharp distribution of the relaxation time of PBMA,[27] increasing the homogeneity of polymer. Studies have shown that the addition of small molecules that H-bonded with polymer occupies part of the free volume, which may accelerate the glass transition process and shorten the relaxation time, thereby decreasing peak width.[28] Second, the β_{JG} process of PBMA can be suppressed when strong intermolecular hydrogen bonding exists in polymer/small molecule blends,[18–20] which may decrease the peak width of PBMA. This part of work should be further verified by dielectric analysis in the future.

Comparison of the five hybrid systems indicates that small molecule selection must consider the following factors. First, a hindered group beside the hydroxyl is indispensable for mediation

of hydrogen bond strength. Second, the crystalline ability of the small molecules must also be relatively weak, which is beneficial to the damping property and enhances the stability of the final material.

CONCLUSION

In this study, the influences of hydrogen bonding interactions on the T_g of PBMA and damping properties of PBMA/small molecule hybrid materials were evaluated. Results showed that the T_g observed for strong hydrogen bonding systems demonstrates positive deviations, whereas weakly hydrogen bonding systems reveal Fox variations. The damping properties of five materials were improved. The loss factor and TA value of relatively weak hydrogen bonding systems showed substantial improvement.

ACKNOWLEDGMENTS

This research was supported by grants from the "973" project (2013CB035505), the National Natural Science Foundation of China (51373053), and the Fundamental Research Funds for the Central Universities.

REFERENCES

1. Wu, C.; Yamagishi, T. A.; Nakamoto, Y.; Ishida, S. I.; Nitta, K. H.; Kubota, S. *J. Polym. Sci. Part B: Polym. Phys.* **2000**, *38*, 1341.
2. Wu, C.; Yamagishi, T. A.; Nakamoto, Y.; Ishida, S. I.; Nitta, K. H. *J. Polym. Sci. Part B: Polym. Phys.* **2000**, *38*, 2943.
3. Xiang, P.; Zhao, X. Y.; Xiao, D. L.; Lu, Y. L.; Zhang, L. Q. *J. Appl. Polym. Sci.* **2008**, *109*, 106.
4. Akasaka, S.; Shimura, T.; Sasaki, S.; Tominaga, Y.; Asai, S.; Sumita, M. *Compos. Interfaces* **2005**, *12*, 637.
5. Ding, X. B.; Zhang, H. P.; Yan, X. *J. Mater. Sci.* **2009**, *44*, 2683.
6. Cao, Y.; Shen, F.; Mou, H.; Cao, D.; Xu, H.; Wu, C. *Polym. Eng. Sci.* **2010**, *50*, 2375.
7. Hu, T.; Bo, Q.; Zhao, X. Y.; Wu, S. Z. *Adv. Mater. Res.* **2012**, *410*, 313.
8. Xu, K.; Zhang, F.; Zhang, X.; Hu, Q.; Wu, H.; Guo, S. *J. Mater. Chem. A* **2014**, *2*, 8545.
9. Zhang, J.; Wang, L.; Zhao, Y. *Polym. Compos.* **2012**, *33*, 2125.
10. Liu, Q. X.; Ding, X. B.; Zhang, H. P.; Yan, X. *J. Appl. Polym. Sci.* **2009**, *114*, 2655.
11. Li, C.; Xu, S.-A.; Xiao, F.-Y.; Wu, C.-F. *Eur. Polym. J.* **2006**, *42*, 2507.
12. Zhao, X.-Y.; Xiang, P.; Tian, M.; Fong, H.; Jin, R.; Zhang, L.-Q. *Polymer* **2007**, *48*, 6056.
13. Song, M.; Zhao, X.; Li, Y.; Hu, S.; Zhang, L.; Wu, S. *RSC Adv.* **2014**, *4*, 6719.
14. Paudel, A.; Nies, E.; Van den Mooter, G. *Mol. Pharm.* **2012**, *9*, 3301.
15. Mugica, A.; Calahorra, M.; Cortazar, M. *Macromol. Chem. Phys.* **2002**, *203*, 1088.
16. Garwe, F.; Schonhls, A.; Lockwenz, H.; Beiner, M.; Schoter, K.; Donth, E. *Macromolecules* **1996**, *29*, 247.
17. Nagi, K. L.; Gopalakrishnan, T. R.; Beiner, M. *Polymer* **2006**, *47*, 7222.
18. Lei, D.; Runt, J.; Safari, A.; Newnham, R. E. *Macromolecules* **1987**, *20*, 1797.
19. Zhang, S.; Jin, X.; Painter, P.; Runt, J. *Macromolecules* **2003**, *36*, 7179.
20. Atorngitjawat, P.; Klein, R. J.; McDermott, A. G.; Masser, K. A.; Painter, P. C.; Runt, J. *Polymer* **2009**, *50*, 2424.
21. Zhao, Y.; Inbar, P.; Chokshi, H. P.; Malick, A. W.; Choi, S. *J. Pharm. Sci.* **2011**, *100*, 3196.
22. He, Y.; Zhu, B.; Inoue, Y. *Prog. Polym. Sci.* **2004**, *29*, 1021.
23. Coates, J. Encyclopedia of Analytical Chemistry; Wiley Online Library: New York, **2000**.
24. Stuart, B. Kirk-Othmer Encyclopedia of Chemical Technology; Wiley Online Library: New York, **2005**.
25. He, Y.; Asakawa, N.; Inoue, Y. *J. Polym. Sci. Part B: Polym. Phys.* **2000**, *38*, 1848.
26. Liu, C.; Yin, X.; Lin, Y.; Guan, A.; Wu, G. *J. Polym. Sci. Part B: Polym. Phys.* **2014**, DOI: 10.1002/polb.23642.
27. Wu, C.; Yamagishi, T. A.; Nakamoto, Y.; Ishida, S. I.; Kubota, S.; Nitta, K. H. *J. Polym. Sci. Part B: Polym. Phys.* **2000**, *38*, 1496.
28. Qiao, B.; Zhao, X.; Yue, D.; Zhang, L.; Wu, S. *J. Mater. Chem.* **2012**, *22*, 12339.